ACS MATERIALS LETTERS

www.acsmaterialsletters.org

PERSPECTIVE

A Perspective on Protective Carbon Shells for Improved Stability of Alkaline Water Oxidation Electrocatalysts

Published as part of ACS Materials Letters virtual special issue "Materials for Water Splitting".

Lettie A. Smith, Kenta Kawashima, Raul A. Marquez, and C. Buddie Mullins*

Cite This: *ACS Materials Lett.* 2024, 6, 3190−3201

Read Online

ACCESS | Metrics & More | Article Recommendations | Supporting Information

ABSTRACT: In recent years, carbon shells have garnered attention as possible protective layers that can be applied to oxygen evolution reaction (OER) electrocatalysts to prevent corrosion under alkaline conditions. However, thermodynamic considerations and experimental results indicate that these carbon shells are subject to corrosion themselves, limiting their applicability as protective coatings against oxidation. Herein, the thermodynamics of carbon corrosion are presented with spectrometric, spectroscopic, crystallographic, microscopy, and electrochemical measurements, emphasizing the inevitable degradation of carbon under alkaline OER conditions. Recent work focused on suppressing this carbon corrosion is then discussed alongside future directions for carbon shells in water oxidation research.

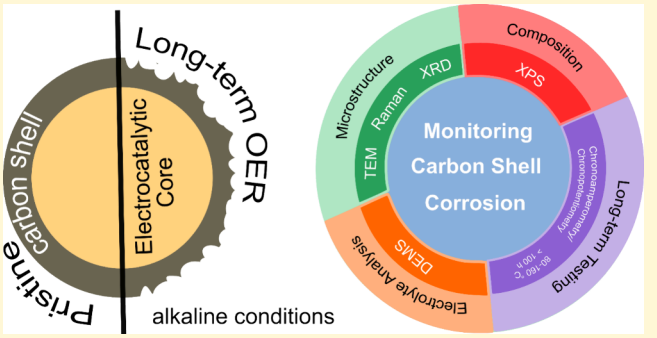

The increasing threat of climate change on human health and the global economy has reinvigorated the development of alternative energy technologies globally.[1,2] Of these technologies, alkaline water electrolyzers are of interest, as they enable the generation of hydrogen fuel (H_2) via the splitting of water without emitting CO_2, unlike the current primary method for H_2 generation: steam methane reforming of natural gas.[3] While promising, water electrolysis is limited by polarization losses incurred by electrolyte leakage, slow kinetics, and corrosion of cell components.[4,5] This corrosion is especially concerning at the anode, the electrode at which water oxidation occurs, within the water electrolyzer cell. In the literature, electrode materials for oxygen evolution reaction (OER) electrocatalysis at the anode have been studied extensively in an effort to boost electrocatalytic activity, but are typically subjected to oxidation, leading to surface transformation and material dissolution after long-term testing using chronoamperometry, chronopotentiometry, or cyclic voltammetry cycling.[6,7] The oxidation of these electrocatalytic materials calls into question their long-term stability and potential as anode materials in industrial water electrolyzers.

Recently, researchers have begun to employ carbon shells to protect electrocatalytic OER core structures from oxidation under alkaline conditions. Essentially, the carbon shell can limit electrolyte contact with the electrocatalytic core, while also imparting improved electrical conductivity, increased electrochemically active surface area, and providing additional active sites for OER electrocatalysis.[8−14] These carbon shell−core materials have been implemented as metal and transition metal nanoparticles encased in carbon, including metal carbides, metal phosphides, metal sulfides, MXenes, and other unique structures.[9−19,19−27] While the carbon shells for these materials are reported as imparting stability, thermodynamic consider-

> In recent years, carbon shells have garnered attention as possible protective layers that can be applied to oxygen evolution reaction (OER) electrocatalysts to prevent corrosion under alkaline conditions.

Received: March 28, 2024
Revised: June 10, 2024
Accepted: June 11, 2024

ations and recent studies on carbon corrosion contradict this finding.[28−33]

This perspective discusses recent work concerning the validity of carbon shells as protective layers against OER electrocatalyst oxidation under alkaline conditions. Specifically, the thermodynamics of carbon corrosion are presented alongside spectrometric, spectroscopic, crystallographic, microscopy, and electrochemical measurements pointing to the inevitable corrosion of carbon under alkaline OER conditions. The future of carbon in conjunction with OER electrocatalysts is then presented based on recent studies, namely that carbon as a protective layer against oxidation should be assumed to be sacrificial unless intensive structural engineering has been implemented to limit the extent of carbon corrosion.[28,34,35]

This perspective discusses recent work concerning the validity of carbon shells as protective layers against OER electrocatalyst oxidation under alkaline conditions.

ditions (pH > 13), thermodynamics indicate that the standard potential required for the OER is E^0 = 1.23 V vs the reversible hydrogen electrode (V_{RHE}) or 0.402 V vs the standard hydrogen electrode (V_{SHE}) and that the standard potentials corresponding to carbon corrosion to CO_2 and CO are E^0 = 1.04 V_{RHE} (0.207 V_{SHE}) and E^0 = 1.35 V_{RHE} (0.518 V_{SHE}) (eqn. 1 and 2), respectively.[28,29] At high, positive potentials (1.35 V_{RHE} or greater) generated CO will immediately oxidize to CO_2 (0.725 V_{RHE}, −0.103 V_{SHE}, eqn. 3) and, in the presence of KOH, produced CO_2 will immediately convert to CO_3^{2-} (eqn. 4). This electrochemical corrosion of carbon is dependent on pH as indicated by the Pourbaix diagram in Figure 1.[36−38] As shown in the Pourbaix diagram, at pH of 14, and potentials > 0.402 V_{SHE} (1.23 V_{RHE}) for catalysis of the OER, carbon will oxidize to CO_3^{2-} as expected.

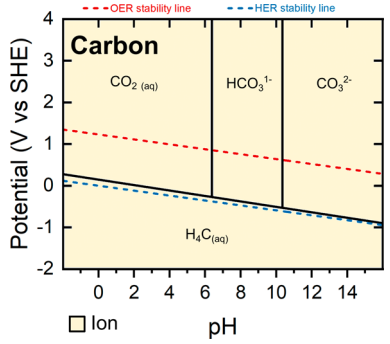

Figure 1. Pourbaix diagram for carbon using the default ion concentration within the Materials Project database.[36−38] The dashed red and blue lines represent the thermodynamic potential for the hydrogen evolution reaction and the OER.

$$C_{(s)} + 2H_2O \rightarrow CO_2 + 4H^+ + 4e^- \ (E^0 = 0.207\ V_{SHE}) \quad (1)$$

$$C_{(s)} + H_2O \rightarrow CO + 2H^+ + 2e^- \ (E^0 = 0.518\ V_{SHE}) \quad (2)$$

$$CO_{(g)} + H_2O \rightarrow CO_2 + 2H^+ + 2e^- \ (E^0 = -0.103\ V_{SHE}) \quad (3)$$

$$2OH^- + CO_2 \rightarrow CO_3^{2-} + H_2O \quad (4)$$

Experimental evidence of this corrosion has been found via monitoring carbon corrosion products with differential electrochemical mass spectrometry (DEMS).[29,30] For example, by employing DEMS, Möller and co-workers monitored carbon corrosion in alkaline electrolyte via direct CO_2 detection through the acidification of generated CO_3^{2-} back to CO_2. The authors discussed how the oxidation of carbon to CO_2 contributes to the Faradaic response observed for the OER (Figure 2a). When comparing carbon corrosion of a graphite electrode under acidic (pH = 1) and alkaline (pH = 13, 0.1 M KOH) conditions following chronopotentiometry at an applied current density of 5.5 mA•cm^{-2}, they found that the CO_2 signal dropped ∼ 82% as the pH increased from 1 to 13 (Figure 2c).[29] This result indicated that carbon corrosion occurs under alkaline conditions, but to a much lesser extent as compared to acidic environments. Additional chronopotentiometric measurements of Vulcan XC 72 carbon (Vulcan) and Ni_xB supported on Vulcan at 10 wt% (Ni_xB/C-10) at various applied current densities (4.4, 8.8, 13.3, 17.7 mA•cm^{-2}), found that carbon oxidation was suppressed when the carbon support was homogeneously covered by the Ni_xB catalyst,[29] meaning that carbon corrosion was only halted when it was no longer exposed to the electrolyte. Thus, protective carbon layers on OER electrocatalysts, much like carbon supports, are subject to oxidation during the electrocatalysis of the OER at high pH and oxidizing potentials. And, as Möller *et al.* showed, the exposure of carbon to these harsh conditions can lead to the loss of carbon atoms in the form of CO_2 which will convert to CO_3^{2-} in solution as prescribed by the Pourbaix diagram of carbon (Figure 1).

Beyond DEMS analysis of a graphitic working electrode, further evidence of carbon corrosion has been observed from the analysis of the electrolyte and a carbon electrocatalyst post-OER testing using transmission electron microscopy, spectrophotometry (photoluminescence, ultraviolet−visible spectrophotometry, infrared spectrophotometry), and N_2 porosimetry. Specifically, Wu and co-workers found that their carbon fiber cloth treated at 450 °C suffered in terms of stability after applying static potentials [1.375, 1.454. 1.725, and 1.935 V vs reversible hydrogen electrode (V_{RHE})] for 1 h each.[31] As shown in Figure 3, with increasing potential, the color of the electrolyte became opaque and eventually turned a dark brown after being held at 1.935 V_{RHE} for 1 h. They attributed this color change to the loss of carbon from the carbon fiber cloth as carbon nanodots. Transmission electron microscopy (TEM) images confirmed the presence of these carbon nanodots in the electrolyte. As shown in Figure 3, dots were visualized from each sample of electrolyte taken after each static potential hold. The detected lattice spacing of 0.247 nm confirmed these dots were carbon, as this spacing corresponds to the (100) plane of graphitic carbon (Figure 3a). As the potential increased, the size of the carbon nanodots increased and the morphology eventually changed to ultrathin graphene nanosheets. From photoluminescence emission spectra of the electrolyte samples, there was also a clear red-shift in peak position (511 to 530 nm) with increasing static potential, indicative of an increasing size of the nanodots with more positive potential, affirming the TEM analysis of the electrolyte. Additionally, scanning electron

https://doi.org/10.1021/acsmaterialslett.4c00688
ACS Materials Lett. 2024, 6, 3190−3201

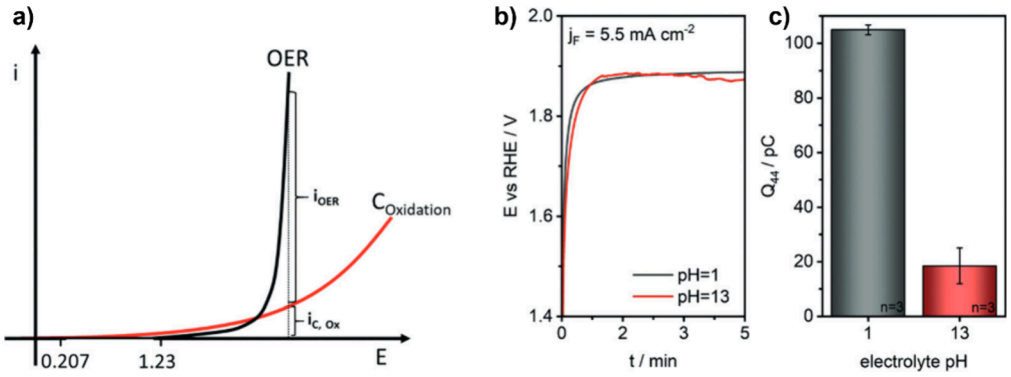

Figure 2. Online-monitoring of carbon corrosion under alkaline OER conditions. (a) Schematic of carbon corrosion contribution to the OER current, (b) Potential response of a graphite electrode at an applied current density of 5.5 mA•cm^{-2} under acidic and alkaline conditions, (c) bar chart showing the corresponding ion charge detected for CO_2, indicative of the loss of C from the electrode at different pH. Reprinted with permission under a Creative Commons CC-BY 4.0 license from ref 29. Copyright 2020 Wiley.

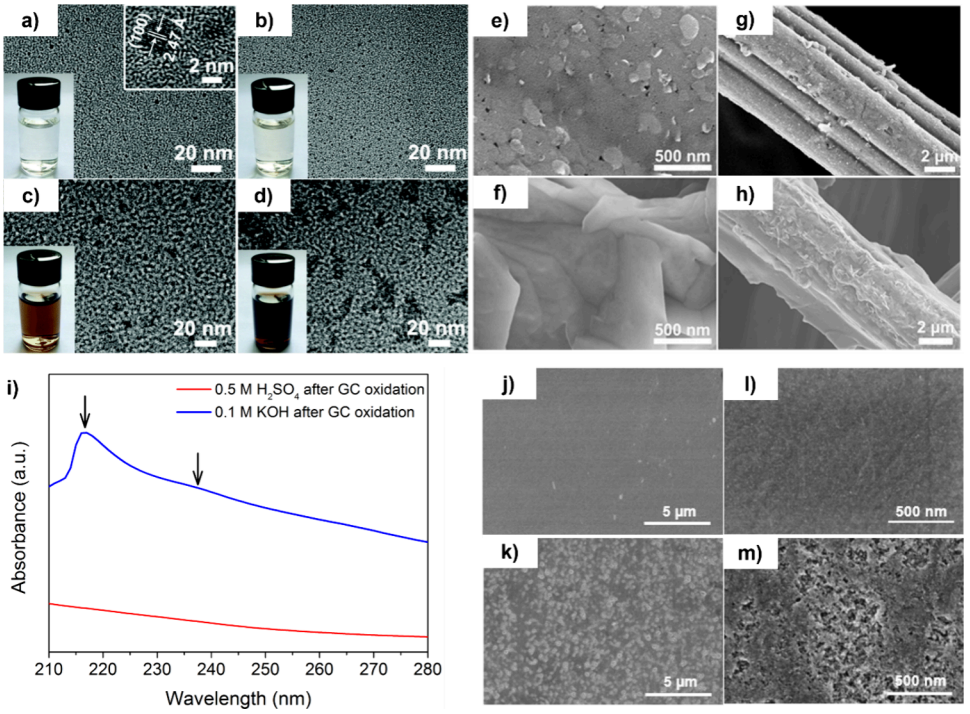

Figure 3. Bulk carbon corrosion. TEM images and samples of the electrolyte after applying (a) 1.375, (b) 1.454, (c) 1.725, and (d) 1.935 V_{RHE} to carbon fiber cloth treated at 450 °C, SEM images of the carbon cloth after applying (e,g) 1.375 V_{RHE} and (f,h) 1.935 V_{RHE}. Used with permission of Royal Society of Chemistry from ref 31. Copyright 2019 Royal Society of Chemistry; permission conveyed through CCC, Inc. (i) UV−vis spectra of the electrolyte after oxidation of glassy carbon (GC) at 1.8 V_{RHE} in alkaline and acidic media, (j,l) pristine GC, (k,m) GC after exposure to alkaline electrolyte. Reprinted with permission under a Creative Commons CC-BY 4.0 License from ref 28. Copyright 2017 Elsevier.

microscopy (SEM) images of the carbon fiber cloth taken after static potential holds showed pore generation and the emergence of nanosheets at the surface with increasing potential, signaling that carbon degradation had occurred (Figure 3e-h). This degradation was further confirmed by N_2 porosimetry after applying 1.375 V for 1 h to the carbon fiber cloth, as the pore volume and surface area increased 990x and 41x, respectively. This increase in pore volume and surface area was a clear indication that the carbon surface had undergone oxidation, leading to a more porous structure. Wu *et al.* determined that the degradation increased with increasing potential and resulted in nanosheets rather than carbon nanodots because of the exfoliation of carbon nanosheets from the carbon fiber cloth. Specifically, hydroxyl radicals from the oxidation of water first attacked edge sites and defect sites on the carbon sheets making up the carbon cloth. At low potentials (1.375 and 1.454 V), this resulted in the loss of carbon as nanodots. With increasing potential (up to 1.935 V), the abundance of hydroxyl radicals increased, leading to further oxidation past the edge sites. This oxidation resulted in increased *d*-spacing between the sheets until, eventually, exfoliation occurred and graphene nanosheets were lost to the electrolyte. Thus, by using a variety of techniques, Wu and co-workers were able to trace the extent of carbon corrosion with the applied potential and conclude that carbon corrosion can

https://doi.org/10.1021/acsmaterialslett.4c00688
ACS Materials Lett. 2024, 6, 3190−3201

only be minimized at low overpotentials for the OER (~1.3−1.4 V).

In addition to Wu and co-workers, the effect of potential on carbon corrosion has been noted by others,[28,39−43] specifically that past a threshold potential (>~1.5 V_{RHE}), instead of simply oxidizing the surface of carbon, C atoms will be removed from the surface as CO and CO_2 (CO_3^{2-} in presence of KOH). In a study of the electrochemical oxidation of glassy carbon, Yi *et al.* observed that carbon oxidation began at 1.2 V in 0.1 M KOH. Additionally, they observed an increase in capacitance from 0.3 mF/cm^2_{geo} to ~ 1.0 mF/cm^2_{geo} from 0 to 5 h of exposure to oxidizing potentials. The capacitance then stabilized around ~ 1.1 mF/cm^2_{geo} from 5 to 25 h.[28] This increase in capacitance resulted from the generation of a porous surface via electrochemical oxidation. Additionally, the electrolyte turned brown after extensive exposure to high anodizing potentials. Analysis of the electrolyte using UV−vis confirmed that carbon had dissolved into the electrolyte via detection of a peak at ~ 220 nm with a shoulder at 235 nm, which corresponds to that of carbon nanodots (<10 nm in diameter) (Figure 3i). Scanning electron microscopy images confirmed this dissolution via the presence of pitting in the electrode after applying 1.8 V_{RHE} for several hours (Figure 3j-m). Further characterization of the glassy carbon electrode using Raman spectroscopy, infrared spectroscopy, and X-ray photoelectron spectroscopy (XPS) indicated that the oxidation of glassy carbon under alkaline conditions was confined to the surface. Specifically, no changes were observed between the Raman spectra or the IR spectra for pristine GC and GC exposed to alkaline conditions. From analysis of the high-resolution O1s XPS spectra, an increase in the peak corresponding to carbonyl groups was observed, indicating that oxidation was limited to within 8−10 nm of the surface. Yi and co-workers hypothesized that the oxidation of the electrode occurred via OH radicals interacting with alkyl chains at the edges of graphitic domains in the glassy carbon. Thus, increasing oxidation resulted in the disruption of π-π interactions between graphitic sheets and the loss of carbon to the electrolyte.[28] Given glassy carbon is considered relatively inert, the oxidation of its surface as confirmed here via a variety of techniques indicates that protective carbon shells formed around electrocatalytic cores are likely subjected to similar if not more extensive oxidation.

In the literature, evidence of this instability of protective carbon shells encapsulating OER electrocatalysts is hinted at; however, rarely investigated or discussed in detail. For example, Abbas and co-workers concluded that their N-doped carbon-protected Fe_3C nanoparticles (NP) were stable upward of 10 h after performing chronoamperometry at 1.7 V_{RHE} in 0.1 M KOH.[14] Diffraction patterns before and after long-term testing provided further evidence of this 'protective' carbon as there were no changes in the diffraction patterns (Figure 4a). Additionally, TEM images taken after long-term testing showed that there was no change to the morphology of the electrocatalysts, including no observable particle agglomeration (Figure 4b). However, Abbas *et al.* did detect a small amount of CO_2 at the surface of the electrode, which they attributed to carbon oxidation. They did not explain how they detected this CO_2. From a C-site poisoning experiment of the Fe_3C@C-N, wherein they used an electrolyte of NaH_2PO_4 (0.1 M) in addition to KOH (0.1 M) to provide phosphate anions, which have a preference for C atoms over OH^-, they observed a dramatic drop in electrocatalytic performance. This result implies that the N-doped carbon shell contributes to the

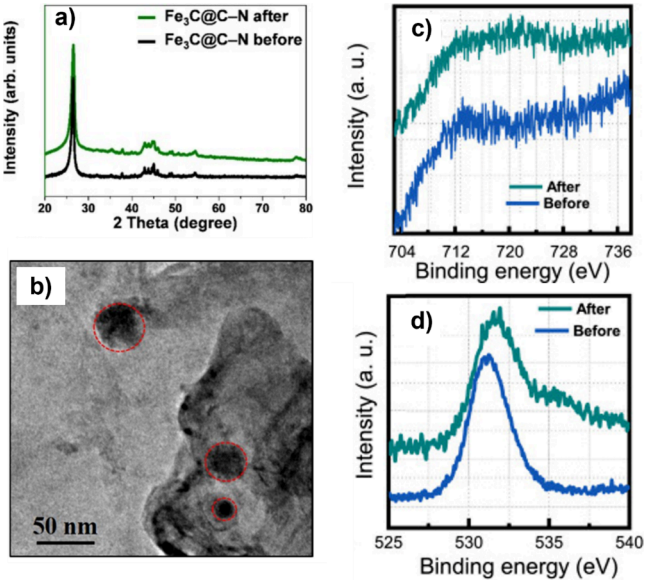

Figure 4. Protective carbon shells on iron carbide cores. (a) XRD of Fe_3C@C-N before and after long-term testing, (b) HR-TEM of Fe_3C@C-N after stability testing, wherein the red dashed circles indicate the Fe_3C NPs. Reprinted from ref 14., Copyright 2021, with permission from Elsevier. High-resolution XPS spectra of (c) Fe 2p, and (d) O1s for FO_{800}. Reprinted from ref 10., Copyright 2022, with permission from Elsevier.

electrocatalytic activity of the catalyst via favorable OH^- adsorption. Bandal and co-workers reached a similar conclusion via the poisoning of Fe sites using thiocyanate, followed by the poisoning of C sites with PO_4^{3-} of their N-doped carbon-coated Fe_3C NPs prepared at 800 °C.[10] Specifically, neither the Fe-sites nor the carbon sites alone accounted for the activity of their electrocatalyst. Rather, the interaction of the Fe_3C core and carbon shell made its low overpotential of 330 mV possible because it led to an increase in the electron density for improved charge transfer, as determined via Mott−Schottky analysis. The adsorption of OH^- at C-sites indicates that oxidation of the carbon layer is occurring. Additionally, Bandal *et al.* found that the Fe_3C core of their material underwent surface oxidation following a 50 h chronoamperometry test at 1.56 V_{RHE}.[10] The Fe(0) peak in the Fe 2p high-resolution XPS spectra disappeared following chronoamperometry and all the peaks in the O 1s spectra shifted to more positive binding energies, indicative of oxidation (Figure 4c and d). Additionally, a new peak emerged in the O 1s spectra at 535.6 eV indicative of chemisorbed OH (Figure 4d). And, while they did not observe a morphological change in their material, it is still possible that carbon flaked off as sheets into the electrolyte, leaving behind a similar surface to that of the starting material. Thus, as for bulk carbon materials, carbon layers surrounding electrocatalytic cores are also subject to oxidation and the oxidation of these layers could eventually lead to cracks such that the electrolyte will come into contact with the electrocatalytic core.

Many reports point to the stability of electrocatalytic cores protected by carbon shells solely on the basis of a stable chronoamperometric or chronopotentiometric response. However, these 'stable' responses are often only observed over a short period of time or do not capture possible material transformation at the surface of electrocatalytic materials or protective carbon shells encapsulating electrocatalytic cores.[20,31] For example, Tao and co-workers found that a 7

https://doi.org/10.1021/acsmaterialslett.4c00688
ACS Materials Lett. 2024, 6, 3190−3201

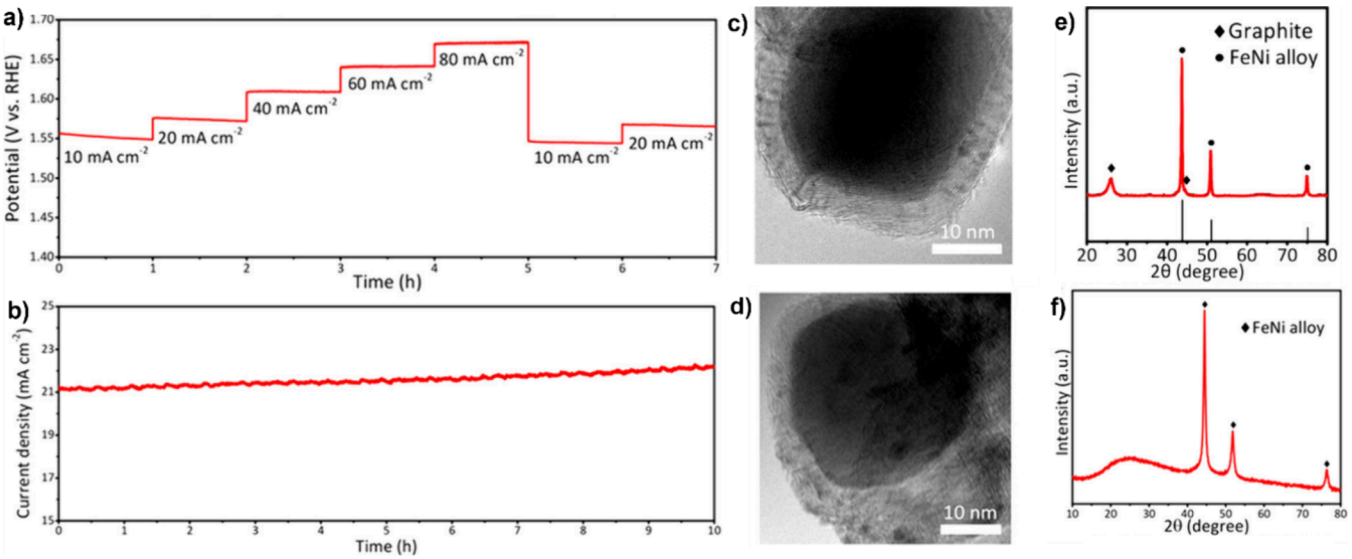

Figure 5. Characterization results of NiFe alloy embedded in N-doped CNTs. (a) chronogalvanostatic stability measurements, (b) CA at 1.56 V_{RHE}, TEM image (c) before and (d) after long-term OER testing, XRD patterns (e) before and (f) after long-term OER testing. Reprinted with permission from ref 21. Copyright 2016 American Chemical Society.

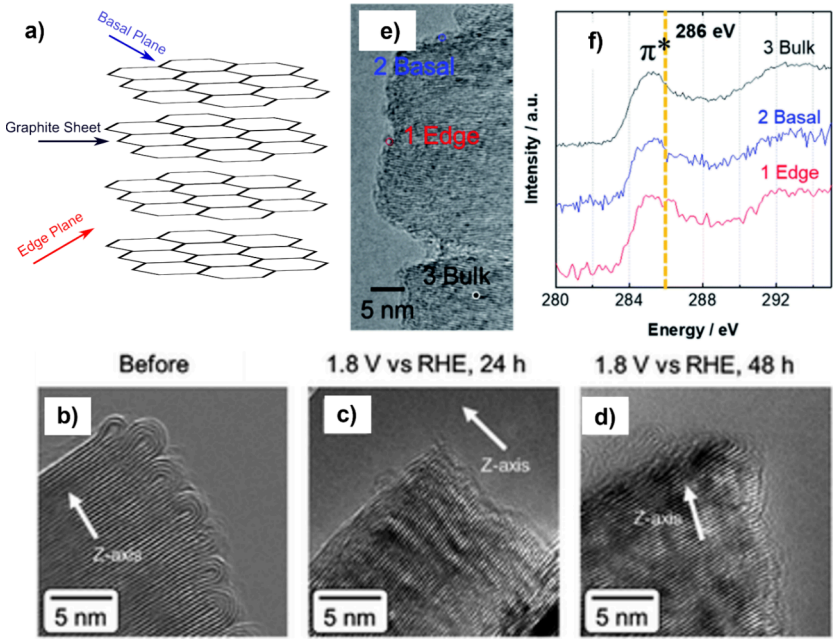

Figure 6. Microstructure and carbon stability. (a) Schematic of stacked graphite sheets, showing the edge and basal planes, TEM of (b) as-prepared pCNF prepared at 2400 °C, (c) after 24 h of CA at 1.8 V_{RHE}, (d) after 48 h of CA at 1.8 V_{RHE}, (e) STEM image of pCNF prepared at 2400 °C, (f) corresponding C-K edge of core-loss EEL spectrum taken after 24 h of CA at 1.8 V_{RHE}. Used with permission of Royal Society of Chemistry from ref 49., Copyright 2021 Royal Society of Chemistry; permission conveyed through CCC, Inc.

nm thick carbon shell imparted optimal stability for their FeNi alloy NPs embedded in N-doped CNTs.[21] This stability of the core was; however, at the expense of the carbon shell. Post-characterization using TEM, XPS, and XRD showed that there was no transformation to the core after long-term testing via chronogalvanostatic measurements at various current densities and chronoamperometry at 1.56 V for 10 h (Figure 5a and b). As shown in Figure 5d, the TEM image post-long-term testing indicated that the core−shell structure of the FeNi alloy NPs embedded in N-doped CNTs was maintained. Then, as for the pristine material, no signal was detected with respect to Fe or Ni via XPS, providing evidence that the core was still completely covered by its carbon shell. In addition, all diffraction peaks for the FeNi alloy and that corresponding to the (002) plane of graphite were retained following long-term OER (Figure 5e and f). However, the (002) peak broadened following long-term OER, indicative of a loss of crystallinity in the carbon shell (Figure 5f), which was likely the result of carbon oxidation via contact with the electrolyte. Further evidence of this carbon corrosion is seen by the (002) peak shift to a lower 2θ (from ~ 25.5° to ~ 24.7°) after long-term testing (Figure 5f). This peak shift means that the d-spacing increased between the graphitic carbon sheets, likely owing to the breaking of π-π interactions due to the presence of OH^-, as postulated for bulk carbon by

https://doi.org/10.1021/acsmaterialslett.4c00688
ACS Materials Lett. 2024, 6, 3190−3201

others.[31] In addition, this transformation of the carbon shell could explain the 1% increase in the current response, which the authors hypothesized could be the result of an activation process (Figure 5b). Thus, the carbon shell protected the FeNi alloy core from the oxidizing environment of the alkaline electrolyte, but at the expense of its own structural stability.

In 1988, Ross and Sattler found that the microstructure of highly graphitized carbon led to improved corrosion resistance compared to non-graphitized carbon under OER conditions (30% KOH, 55 °C).[35] They graphitized furnace carbon blacks at 2700 °C for 2 h under a helium atmosphere and subjected them to long-term OER (15 h at 0.450 $V_{Hg/HgO}$ followed by 5 h at 0.550 $V_{Hg/HgO}$) alongside their as-received counterparts. The graphitized carbon blacks demonstrated a reduced corrosion rate (0.02 to 0.5% h^{-1}) compared to the as-received carbon blacks (0.1 to > 10%·h^{-1}), as determined by correcting the anodic current for OER current contributions using mass spectrometry and converting the corrosion current using Faraday's law. From TEM and XRD results, the graphitized carbons demonstrated increased crystallinity and an increased coherence length along (002) (L_c) as compared to their non-graphitized counterparts.[44] Chemisorption experiments using iodine indicated that the microstructure of the graphitized carbon blacks explained their corrosion resistance. Graphitic carbon consists of stacked graphite sheets consisting of basal and edge planes (Figure 6a). When exposed to iodine, the graphitized carbons with increased order, attributable to the basal plane of graphite, had reduced iodine adsorption as compared to the non-graphitized carbons. As the non-graphitized carbon blacks had no basal plane area, increased iodine adsorption and an increased rate of corrosion, Ross and Sattler concluded that the iodine adsorbed preferentially to favorable oxidation sites. And, as the non-graphitized carbons consisted of amorphous domains and edge sites, a less ordered microstructure was attributed to increased corrosion.

Recent studies have further explored the effect of the carbon microstructure on stability under OER conditions with multiple reports confirming that oxidation occurs initially at the edge planes of graphitic carbon and/or at amorphous sites.[43,45−48] With this knowledge, researchers have begun further investigating the oxidation at the basal plane vs the edge plane and amorphous domains. For example, Sato *et al.* found that their platelet-type carbon nanofibers (pCNFs), despite largely consisting of edge planes of graphite, had reduced corrosion resistance at the edge because of the passivation of the edge planes with hydroxyl species.[49] The pCNFs consisted of a nanofiber with carbon sheets, or platelets, normal to the nanofiber axis connected by carbon loops. This morphology resulted in basal planes of carbon at the ends of the nanofibers, exposed to the electrolyte, and edge planes along the fiber (Figure 6b). As Ross *et al.* and others have found, Sato and co-workers observed that the corrosion rate decreased with increased graphitization of the pCNFs. Specifically, they found that as the heat treatment of the pCNFs went from 2000 to 2400 to 3000 °C, the spacing between the stacked carbon sheets (d_{002}) decreased, approaching that of graphite at ∼ 0.34 nm. From an identical-location scanning electron microscopy technique, wherein they compared SEM images of the same point on the pCNFs before and after long-term testing at a potential of 1.8 V_{RHE} for 24 and 48 h, they were able to determine the corrosion rate at the basal plane via monitoring changes in pCNF length. For the samples prepared at 2000, 2400, and 3000 °C, respectively, the basal plane corrosion rates were 0.62, 0.42, and 0.34 nm•h^{-1}. Interestingly, the same measurements at the edge planes showed only negligible corrosion, contrary to previous reports.[35,45] TEM and scanning transmission electron microscopy (STEM)/electron-energy loss spectroscopy (EELS) provided an explanation for this phenomenon. As shown in Figure 6b-d, the carbon loops that initially covered the edge planes disappeared following long-term OER testing. However, after the loss of the carbon loops, further dissolution of the edge planes was not observed with increasing anodization time (Figure 6d). STEM/EELS detected peaks for the pCNFs at 26 and 16 eV, corresponding to graphite and sp^3-type carbon or oxygen, indicating that functional groups containing oxygen could be retained at the surface. From the K-edge EELS spectra of pCNF prepared at 2400 °C, it was determined that hydroxyl groups were present at the carbon surface via the detection of a peak at 286 eV (Figure 6e and f). As a result, the authors concluded that the lack of corrosion at the edge planes was because of the formation of a passivation layer made up of hydroxyl groups, protecting the carbon underneath. This passivation layer seemed to be unique to the platelet nanofiber structure, evoking the need for additional analysis of the microstructure and its effects on carbon corrosion under alkaline OER conditions.

In addition to Sato and co-workers, Filimonenkov *et al.* also reported a contrary finding to that of Ross and Sattler, and others. From their study of the carbon corrosion of a furnace black (Vulcan XC-72R), acetylene black, and pyrolytic carbon (Sibunit-152) they determined that more ordered carbons experience more corrosion when they are active for OER electrocatalysis. In the comparison of their three carbons, the order increased from Vulcan XC-72R to Sibunit-152 to acetylene black as determined by XRD. Additionally, acetylene black had the largest basal plane coverage followed by Sibunit-152 and Vulcan XC-72R (0.76, 0.62, and 0.48, respectively), as determined from pseudocapacitance measurements. By using a rotating ring disk electrode (RRDE), they were able to isolate current from carbon corrosion and the OER and, as a result, calculate OER efficiency. They found that carbon corrosion increased with decreased structural order only when OER efficiency was low, which occurred at potentials below 1.63 V_{RHE} and above 1.93 V_{RHE}. At intermediate potentials, wherein OER efficiency was high, the opposite trend occurred owing to the increased activity of the carbon toward the OER. TEM images taken after 5 h of OER testing at 1.63V_{RHE} showed degradation of the most ordered material, acetylene black, but negligible changes to the least ordered carbon, Vulcan XC-72R. Additionally, from TEM, there was an increase in d_{002} from 0.35 to 0.5 nm with electrochemical testing time, indicating a clear loss of structural order via oxidation of the carbon from its electrocatalysis of the OER. The authors hypothesize that the less ordered Vulcan XC-72R did not experience extensive oxidation from the OER due to the blocking of its pores via the generation of intermediate species during the OER, as confirmed by the reduction in capacitance with anodization time. Interestingly, when they prepared a composite of their carbons with a metal oxide, they did not detect any material corrosion after 5 h of long-term OER testing. This finding reaffirms the idea of oxygen-containing functional groups as protective against carbon corrosion, as aforementioned in the context of Sato *et al.*'s work and reported by Han and co-workers.[48] Additionally, they postulate that the electrocatalyst employed may affect the durability of carbon. Evidence of this electrocatalyst effect has been demonstrated by Yang *et al.* and their study of $MnCo_2O_4$

https://doi.org/10.1021/acsmaterialslett.4c00688
ACS Materials Lett. 2024, 6, 3190−3201

with carbon black. Specifically, they determined that carbon corrosion could be suppressed when highly active electrocatalysts for the OER are employed, as the fast kinetics of the OER will outcompete the carbon corrosion.[50]

While the analysis of bulk carbon materials has and continues to show that carbon corrosion under alkaline OER conditions will occur, few reports have considered the corrosion of 'protective' layers of carbon encapsulating OER electrocatalysts. Typically, even if post-characterization using techniques such as TEM, XRD, and XPS is performed on these materials, it is only with respect to the core and not the carbon shell.[10,13,21] While the maintained stability of the core is important, that of the carbon 'protecting' the core is also noteworthy because, if the protective layer is not stable, then the long-term stability of the electrocatalytic core is questionable at best. The corrosion of these carbon shells needs to be determined to truly gauge the durability of these materials.

Techniques used to study bulk carbon corrosion need to be applied to the study of these carbon shells to determine their true stability, such as DEMS for CO_3^{2-} detection, XPS to gauge oxidation at the surface via detection of oxygen-containing functional groups, SEM and TEM to observe changes in the morphology, TEM and XRD to track alterations in the microstructure,[35,43] and STEM/EELS to identify oxygen-containing groups at the surface on the basal vs edge plane of ordered carbon.[32] The analysis of carbon shell−core structures using these techniques will provide clear evidence supporting either carbon stability or, more likely, instability. However, these techniques each have challenges associated with them. For example, DEMS can only detect volatile species and special care needs to be taken with regard to calibration of the instrument.[51,52] Concerning XPS, it may also be difficult to discern increased oxidation at the surface because either (1) oxidation of the carbon has resulted in CO_2 evolution that immediately converts to CO_3^{2-} because of the high applied potential and long-term testing or (2) the change in the peaks corresponding to C-O bonds before and after OER testing is minute due to the presence of adventitious carbon.[28,53] Thus, XPS cannot be implemented alone as a post-characterization technique for determining the stability of carbon shell−core OER electrode materials and a combination of techniques should be enlisted. Emphasis should be placed on employing online monitoring, such as through DEMS, or through the use of in situ techniques, especially TEM, as this technique would enable the study of microstructure changes during testing and has demonstrated previous success in the study of structural changes to electrocatalysts.[54,55]

In addition to post and in situ OER testing characterization of the carbon shell−core electrocatalysts, the electrolyte should also be analyzed following long-term testing. Techniques that could aid in the analysis of carbon corrosion products in the electrolyte are DEMS as aforementioned, TEM of degradation products in the electrolyte and spectrophotometric measurements.[28,29] Regarding spectrophotometry, carbon nanodots with photoluminescent properties have been detected as carbon degradation products, which can be detected using fluorimetry and UV−vis spectrophotometry.[28,31,56] In addition to these methods, inductively coupled plasma mass spectrometry (ICP-MS) has also been employed to detect dissolution products in the electrolyte of oxidized OER electrocatalysts. However, for the study of carbon corrosion, ICP-MS is not recommended because C-species are difficult to detect accurately due to possible environmental contamination during sample preparation and because carbon exists as an impurity in the plasma.[57] An alternative method that could be implemented to indirectly trace sample loss to the electrolyte is combustion analysis, which enables the quantification of carbon content via the combustion of a solid material. However, this method, as with ICP-MS, is subject to carbon contamination from the environment.[58] Thus, if this technique were to be implemented, only the ratio of C to another detectable element using this technique, such as N, should be compared before and after long-term testing. In general, analysis of the electrolyte can be challenging, as detected CO_3^{2-} could also originate from the electrocatalytic core for materials such as metal carbides.[6] To circumvent this challenge, it is recommended to prepare control samples without a carbon shell as a standard for comparison.

Because many carbon shells form around a metal or transition metal core in situ,[6] the synthesis of control samples without a carbon shell is challenging, but vital. Such controls are needed to gauge the extent to which carbon shells can suppress electrocatalytic core oxidation and to measure the oxidation of the shell itself, as aforementioned. Thus, methods wherein the carbon shell formation occurs in a separation step or can be prevented while preparing the same core material should be implemented. For example, Pan and co-workers used the solvothermal method to prepare CoS_2 NPs encapsulated in N-doped carbon and bare CoS_2 NPs.[59] Specifically, they added $Co(CH_3COO)_2{\cdot}4H_2O$ and thiourea to ethylene glycol, stirred the mixture (0.5 h, 50 °C), added the surfactant CTAB as a structure guiding agent, and then added glucose as the carbon source. After stirring (10 min), they heated the solution in a stainless-steel autoclave (12 h, 180 °C). Sulfur was then incorporated into the structure via calcination using sulfur powder to generate the CoS_2 NPs encapsulated in N-doped carbon. The bare CoS_2 NPs were prepared using the same procedure without the inclusion of glucose. XRD and Raman confirmed that a carbon layer was not present on the bare CoS_2 NPs, as the typical peak at ∼ 26° for carbon was not observed in the diffraction pattern and the D and G-bands indexed to carbon were not observed in the Raman spectrum. Thus, Pan *et al.* were able to prepare a control for comparison to their N-doped CoS_2 NPs.

In addition, Gao *et al.* were also able to prepare Fe_3C NPs with and without a carbon shell, while also regulating the thickness of the carbon shell via changing the Fe precursor identity.[9] They prepared Fe_3C NPs on carbon nanotubes (CNTs) using three separate precursors: ferrous carbonate, iron acetylacetonate, and iron phthalocyanine via microwave-assisted pyrolysis referred to as Fe/Fe_3C-C@CNT, Fe/Fe_3C-A@CNT, and Fe/Fe_3C-P@CNT, respectively. Of the three samples, Fe/Fe_3C-C@CNT did not have a carbon layer coating its Fe_3C NPs while Fe/Fe_3C-A@CNT had a carbon layer with ∼ 1.77 nm thickness and Fe/Fe_3C-P@CNT had a carbon layer thickness of ∼ 9.31 nm. A carbon layer was not observed for Fe/Fe_3C-C@CNT because iron carbonate easily decomposed to CO_2 gas during pyrolysis at 800 °C.[9] They found that Fe/Fe_3C-A@CNT, with a thinner carbon shell, exhibited decreased overpotential by ∼ 50 mV as compared to Fe/Fe_3C-P@CNT with a thicker shell and Fe/Fe_3C-C@CNT without a carbon shell. However, because their Fe_3C NPs with and without a carbon layer varied in size (5 nm to over 200 nm), it is difficult to exclude NP size effects on performance. This work highlights the need for a study in which NP size is held constant while the carbon thickness is varied (or vice versa) to independently determine carbon layer thickness effects with respect to core and shell oxidation under OER

https://doi.org/10.1021/acsmaterialslett.4c00688
ACS Materials Lett. 2024, 6, 3190−3201

conditions. This NP size difference emphasizes the difficulty of making controls without a carbon shell, and introduces additional questions that necessitate further exploration. Specifically, how thick should the carbon layer be to ensure sufficient coverage of the core long-term despite possible carbon corrosion? And then, does increased thickness eventually lead to complete blocking of core active sites?

Reports conflict with regard to the optimal carbon thickness with some reporting a thickness of ∼2−2.5 nm as being best,[9,13] while others indicate that a thicker layer is preferable, but still does not result in complete prevention of oxidation of the electrocatalytic core.[21] For example, Yoo and co-workers observed that a carbon layer thickness up to 3.5 nm led to active site blocking for electrocatalysis,[8] while others have observed decreased overpotential with thicknesses nearing 10 nm (see Table S1). These opposing observations are a result of differing levels of post-characterization analysis of these carbon-coated OER electrocatalysts and long-term testing duration times, which range from hours to hundreds of hours, making it difficult to draw general conclusions with regard to optimal carbon shell thickness.[9,13,14,19,22,24] If a long-term test is only carried out for a few hours and post-characterization is limited, detection of corrosion of both the core and carbon shell could be missed and, as a result, active site blocking via the carbon shell. For example, if only SEM were used, the morphology could go unchanged but changes to the microstructure detectable via XRD and TEM would be overlooked as would the loss of carbon to the electrolyte as CO_3^{2-}. Given the corrosion of carbon has most definitively been traced via monitoring of microstructure changes and the detection of CO_3^{2-}, it is recommended that post-characterization after long-term OER consist, at minimum, of TEM, XRD, and analysis of the electrolyte using DEMS or other aforementioned techniques. As DEMS is typically not readily available, other methods such as using a RRDE to track the corrosion of the carbon with time as Filimonenkov and co-workers demonstrated could also be implemented.[43] Additionally, long-term testing using techniques such as chronoamperometry and chronopotentiometry needs to be extended beyond five to tens of hours.[9,14,19,24] As recommended by Chen *et al.* and demonstrated by others,[60−62] these materials should be tested for at least several hundreds if not thousands of hours to compete with current best-performing OER electrocatalysts in the literature such as NiOOH and porous cobalt phosphide foam, which have demonstrated chronopotentiometric stability up to ∼ 260 and 4000 h, respectively.[61,62] After all, alkaline electrolyzers have lifetimes upward of a decade,[4] meaning for electrocatalysts to be considered 'stable' they should demonstrate lifetimes for at least several weeks to months at the lab scale.

Beyond stability at lab scale in three-electrode systems, the integrity of these carbon shell−core OER electrodes on a larger scale require further evaluation. For future application, scale-up both in terms of the material synthesis and the implementation of these carbon shell−core structures into water electrolyzers warrant investigation. With regard to synthetic scale-up, especially concerning NPs, reproducibility between batches must be considered, as their adaptation into other fields has been limited by variability in their physiochemical properties.[63] Additionally, the reproducibility of the carbon shell must be explored, especially with respect to the microstructure and thickness, as these parameters have implications toward long-term stability of the shell and prevention of the oxidation of the OER electrocatalytic core.

Concerning the incorporation of these carbon-shell core OER electrocatalysts into larger scale devices, specifically lab-scale water electrolyzers, it is likely that carbon corrosion would change under these new conditions. After all, electrocatalytic stability has been shown to change drastically from three-electrode cells to electrolyzers.[62,64] Additionally, as alkaline electrolysis is performed at 80−160 °C,[65] and it has been reported that carbon corrosion is accelerated at elevated temperatures (65 and 90 °C),[66] the study of corrosion with increasing temperature is vital within the context of possible industrial application of protective carbon shells. And, given some carbon corrosion is expected as detailed above, the effect of carbon degradation products on other cell components such as the membrane should also be considered in future work.

The key to the potential implementation of carbon shell−core OER electrocatalysts into water electrolyzers is an understanding of the mechanism of the carbon corrosion at the lab-scale and beyond. As the reports discussed herein indicate, carbon corrosion is unique to the carbon structure and the extent to which it participates in OER electrocatalysis. Thus, as aforementioned, the stability of carbon shells must be thoroughly evaluated in future studies. To summarize, these future studies should incorporate extensive post-characterization (e.g., TEM, XRD, XPS, etc.), incorporating online monitoring and in situ studies (e.g., DEMS, in situ TEM) when possible, and testing of carbon core−shell electrocatalysts in both three-electrode cells and lab scale electrolyzers under more relevant industrial conditions (e.g., weeks to months of long-term testing at 80−160 °C). Additionally, the role of the carbon shell in OER electrocatalysis should be considered, as reports have indicated that carbon can act as an active site.[10,14,67] It is recommended that future work perform C poisoning experiments via the inclusion of phosphate ions into the electrolyte to gauge the extent that C sites contribute to the OER performance, as demonstrated by Abbas *et al.* and Bandal *et al.* and discussed above.[10,14] This work is instrumental, as carbon is used in other alternative energy devices such as metal-air batteries.[68] In these batteries, the air electrode flips between catalyzing the OER and oxygen reduction reaction for charge and discharge, respectively. Thus, carbon corrosion will occur via exposure to the alkaline electrolyte, the applied potential, and as a result of battery cycling. In Zn-air batteries, this carbon corrosion has been reported to lead to flooding such that the cell efficiency is greatly decreased.[69] Thus, the study of carbon corrosion in electrochemical systems has far-reaching implications.

From both experimental findings and thermodynamic considerations, the inevitable corrosion of carbon under alkaline OER conditions is irrefutable. Thus, when implemented as a 'protective' coating covering OER electrocatalysts, while carbon may prevent oxidation of the electrocatalytic core, this protection is only temporary. The carbon itself will undergo oxidation, likely dissolving completely into the electrolyte as CO_3^{2-} within a matter of weeks.[32] As demonstrated by Sato and co-workers, this oxidation can be suppressed, but not prevented, depending on the microstructure of the carbon. Simply put, just because a carbon layer is graphitic does not mean it will be stable under alkaline OER conditions. The carbon consisting almost entirely of 'corrosion resistance' basal planes will also not provide this stability, as recent studies have shown. The 'protective' carbon layers that have been used to encapsulate OER electrocatalysts need protection from the harsh alkaline electrolyte themselves. Future work should focus on the

https://doi.org/10.1021/acsmaterialslett.4c00688
ACS Materials Lett. 2024, 6, 3190−3201

Future work should focus on the minimization of carbon shell oxidation via structural engineering and the creation of passivation layers at the carbon surface to ensure that these shells can act as long-term protective layers for OER electrocatalytic cores.

minimization of carbon shell oxidation via structural engineering and the creation of passivation layers at the carbon surface to ensure that these shells can act as long-term protective layers for OER electrocatalytic cores. Additionally, when carbon is employed as a coating on electrocatalytic OER materials, it must be strenuously analyzed using post-characterization techniques to definitively determine its role in OER electrocatalysis and the interplay between the carbon and electrocatalyst both in terms of stability and activity.

■ ASSOCIATED CONTENT

Supporting Information

The Supporting Information is available free of charge at https://pubs.acs.org/doi/10.1021/acsmaterialslett.4c00688.

Table summarizing the performance and carbon corrosion of carbon-coated OER electrocatalysts referenced in the manuscript (PDF)

■ AUTHOR INFORMATION

Corresponding Author

C. Buddie Mullins − *Department of Chemistry, McKetta Department of Chemical Engineering, Texas Materials Institute, Center for Electrochemistry, and H2@UT, The University of Texas at Austin, Austin, Texas 78712, United States;* orcid.org/0000-0003-1030-4801; Email: mullins@che.utexas.edu

Authors

Lettie A. Smith − *Department of Chemistry, The University of Texas at Austin, Austin, Texas 78712, United States;* orcid.org/0000-0003-0378-072X

Kenta Kawashima − *Department of Chemistry, The University of Texas at Austin, Austin, Texas 78712, United States;* orcid.org/0000-0001-7318-6115

Raul A. Marquez − *Department of Chemistry, The University of Texas at Austin, Austin, Texas 78712, United States;* orcid.org/0000-0003-3885-5007

Complete contact information is available at: https://pubs.acs.org/10.1021/acsmaterialslett.4c00688

Author Contributions

The manuscript was written through the contributions of all authors. All authors have approved the final version of the manuscript. CRediT: **Lettie A Smith** conceptualization, data curation, investigation, methodology, writing-original draft, writing-review & editing; **Kenta Kawashima** formal analysis, writing-review & editing; **Raul A. Marquez** formal analysis, writing-review & editing; **C. Buddie Mullins** formal analysis, writing-review & editing.

Notes

The authors declare no competing financial interest.

Biographies

Lettie A. Smith received her B.S. in Chemistry from the University of North Carolina at Chapel Hill in Spring 2020. She began graduate school at the University of Texas at Austin in Fall 2020 under the supervision of Prof. C. Buddie Mullins. Her research focuses on electrocatalysis for the ORR, HER, and OER.

Kenta Kawashima received his B.Eng. (2014) and M.Eng. (2016) from Shinshu University. He is currently a Ph.D. candidate (Chemistry) at the University of Texas at Austin. His research focuses on developing highly active electrocatalysts and photoelectrocatalysts for efficient water splitting and exploring the application of a molten-salt synthesis method for studying crystal growth.

Raul A. Marquez received his B.E. in Chemical Engineering (2017) and M.S. in Chemistry (2020) from Universidad Autonoma de Chihuahua, Mexico. He is currently a Ph.D. candidate (Chemistry) at the University of Texas at Austin. His research combines electrocatalysis, analytical chemistry, and electrochemical engineering, with a particular

https://doi.org/10.1021/acsmaterialslett.4c00688
ACS Materials Lett. 2024, 6, 3190−3201

interest in understanding the chemical transformations in energy storage and conversion technologies.

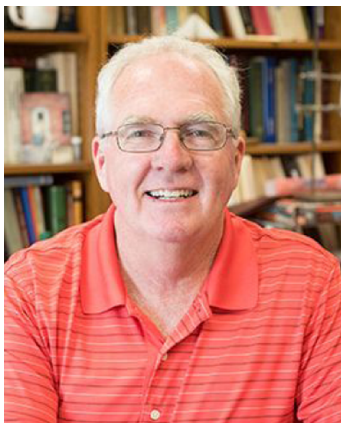

C. Buddie Mullins received a Ph.D. from the California Institute of Technology and was a postdoc at IBM Almaden Research Center. He is currently a Professor in the Departments of Chemical Engineering and Chemistry at the University of Texas at Austin. His interests include surface chemistry, photocatalytic processes, and materials/architectures for advanced batteries.

■ ACKNOWLEDGMENTS

The authors extend their appreciation to the National Science Foundation for their funding support under Grant CHE-2102307, and to the Welch Foundation for their generous assistance through Grant F-1436.

■ REFERENCES

(1) Meckling, J.; Hughes, L. Global Interdependence in Clean Energy Transitions. *Bus. Polit.* **2018**, *20*, 467−491.
(2) th Congress. *The Inflation Reduction Act*; 2022. https://www.congress.gov/bill/117th-congress/house-bill/5376/text.
(3) Cho, H. H.; Strezov, V.; Evans, T. J. Environmental Impact Assessment of Hydrogen Production via Steam Methane Reforming Based on Emissions Data. *Energy Rep.* **2022**, *8*, 13585−13595.
(4) Luo, Y.; Shi, Y.; Cai, N. Bridging a Bi-Directional Connection between Electricity and Fuels in Hybrid Multienergy Systems. In *Hybrid Systems and Multi-energy Networks for the Future Energy Internet*; Elsevier, 2021; pp 41-84. DOI: 10.1016/B978-0-12-819184-2.00003-1.
(5) Shiva Kumar, S.; Lim, H. An Overview of Water Electrolysis Technologies for Green Hydrogen Production. *Energy Rep.* **2022**, *8*, 13793−13813.
(6) Kawashima, K.; Márquez, R. A.; Smith, L. A.; Vaidyula, R. R.; Carrasco-Jaim, O. A.; Wang, Z.; Son, Y. J.; Cao, C. L.; Mullins, C. B. A Review of Transition Metal Boride, Carbide, Pnictide, and Chalcogenide Water Oxidation Electrocatalysts. *Chem. Rev.* **2023**, *123*, 12795−13208.
(7) Vazhayil, A.; Vazhayal, L.; Thomas, J.; Ashok, C. S.; Thomas, N. A Comprehensive Review on the Recent Developments in Transition Metal-Based Electrocatalysts for Oxygen Evolution Reaction. *Appl. Surf. Sci. Adv.* **2021**, *6*, 100184.
(8) Yoo, J. M.; Shin, H.; Chung, D. Y.; Sung, Y.-E. Carbon Shell on Active Nanocatalyst for Stable Electrocatalysis. *Acc. Chem. Res.* **2022**, *55*, 1278−1289.
(9) Gao, T.; Yu, S.; Chen, Y.; Li, X.; Tang, X.; Wu, S.; He, B.; Lan, H.; Li, S.; Yue, Q.; Xiao, D. Regulating the Thickness of the Carbon Coating Layer in Iron/Carbon Heterostructures to Enhance the Catalytic Performance for Oxygen Evolution Reaction. *J. Colloid Interface Sci.* **2023**, *642*, 120−128.
(10) Bandal, H. A.; Pawar, A. A.; Kim, H. Transformation of Waste Onion Peels into Core-Shell Fe_3C@ N-Doped Carbon as a Robust Electrocatalyst for Oxygen Evolution Reaction. *Electrochim. Acta* **2022**, *422*, 140545.
(11) Wang, Z.; Xiao, S.; Zhu, Z.; Long, X.; Zheng, X.; Lu, X.; Yang, S. Cobalt-Embedded Nitrogen Doped Carbon Nanotubes: A Bifunctional Catalyst for Oxygen Electrode Reactions in a Wide pH Range. *ACS Appl. Mater. Interfaces* **2015**, *7*, 4048−4055.
(12) You, B.; Jiang, N.; Sheng, M.; Gul, S.; Yano, J.; Sun, Y. High-Performance Overall Water Splitting Electrocatalysts Derived from Cobalt-Based Metal-Organic Frameworks. *Chem. Mater.* **2015**, *27*, 7636−7642.
(13) Liu, T.; Xiang, Y.; Tan, Z.; Hong, W.; He, Z.; Long, J.; Xie, B.; Li, R.; Gou, X. One-Step Growth of Ni_3Fe-Fe_3C Heterostructures Well Encapsulated in NCNTs as Superior Self-Supported Bifunctional Electrocatalysts for Overall Water Splitting. *J. Alloys Compd.* **2023**, *949*, 169825.
(14) Abbas, S. A.; Ma, A.; Seo, D.; Jung, H.; Lim, Y. J.; Mehmood, A.; Nam, K. M. Synthesis of Fe_3C@C Core-Shell Catalysts with Controlled Shell Composition for Robust Oxygen Evolution Reaction. *Appl. Surf. Sci.* **2021**, *551*, 149445.
(15) Zhang, L.; Xiao, J.; Wang, H.; Shao, M. Carbon-Based Electrocatalysts for Hydrogen and Oxygen Evolution Reactions. *ACS Catal.* **2017**, *7*, 7855−7865.
(16) Zoller, F.; Häringer, S.; Böhm, D.; Luxa, J.; Sofer, Z.; Fattakhova-Rohlfing, D. Carbonaceous Oxygen Evolution Reaction Catalysts: From Defect and Doping-Induced Activity over Hybrid Compounds to Ordered Framework Structures. *Small* **2021**, *17*, 2007484.
(17) Wang, J.; Kong, H.; Zhang, J.; Hao, Y.; Shao, Z.; Ciucci, F. Carbon-Based Electrocatalysts for Sustainable Energy Applications. *Prog. Mater. Sci.* **2021**, *116*, 100717.
(18) Chen, J.; Gao, X.; Li, J.; Kang, Z.; Bai, J.; Wang, T.; Yuan, Y.; You, C.; Chen, Y.; Xia, B. Y.; Tian, X. Progress in MXene-based Catalysts for Oxygen Evolution Reaction. *Electron* **2024**, *2*, No. e17.
(19) Jiang, H.; Yao, Y.; Zhu, Y.; Liu, Y.; Su, Y.; Yang, X.; Li, C. Iron Carbide Nanoparticles Encapsulated in Mesoporous Fe-N-Doped Graphene-Like Carbon Hybrids as Efficient Bifunctional Oxygen Electrocatalysts. *ACS Appl. Mater. Interfaces* **2015**, *7*, 21511−21520.
(20) Zhong, X.; Jiang, Y.; Chen, X.; Wang, L.; Zhuang, G.; Li, X.; Wang, J. Integrating Cobalt Phosphide and Cobalt Nitride-Embedded Nitrogen-Rich Nanocarbons: High-Performance Bifunctional Electrocatalysts for Oxygen Reduction and Evolution. *J. Mater. Chem. A* **2016**, *4*, 10575−10584.
(21) Tao, Z.; Wang, T.; Wang, X.; Zheng, J.; Li, X. MOF-Derived Noble Metal Free Catalysts for Electrochemical Water Splitting. *ACS Appl. Mater. Interfaces* **2016**, *8*, 35390−35397.
(22) Mathew, S.; Kim, J.; Ha, Y.; Li, O. L.; Cho, Y.-R. Hybrid Catalytic-Protective Structure of $CuInS_2$ and B-N Doped Carbon as a Highly Efficient and Ultra-Stable Electrocatalyst for Oxygen Evolution Reaction. *J. Phys. Chem. C* **2021**, *125*, 546−557.
(23) Alsabban, M. M.; Yang, X.; Wahyudi, W.; Fu, J.-H.; Hedhili, Mohamed. N.; Ming, J.; Yang, C.-W.; Nadeem, M. A.; Idriss, H.; Lai, Z.; Li, L.-J.; Tung, V.; Huang, K.-W. Design and Mechanistic Study of Highly Durable Carbon-Coated Cobalt Diphosphide Core-Shell Nanostructure Electrocatalysts for the Efficient and Stable Oxygen Evolution Reaction. *ACS Appl. Mater. Interfaces* **2019**, *11*, 20752−20761.
(24) Zhang, P.; Cai, Z.; You, S.; Wang, F.; Dai, Y.; Zhang, C.; Zhang, Y.; Ren, N.; Zou, J. Self-Generated Carbon Nanotubes for Protecting Active Sites on Bifunctional Co/CoO_x Schottky Junctions to Promote Oxygen Reduction/Evolution Reactions via Efficient Valence Transition. *J. Colloid Interface Sci.* **2019**, *557*, 580−590.
(25) Li, S.; Peng, S.; Huang, L.; Cui, X.; Al-Enizi, A. M.; Zheng, G. Carbon-Coated Co^{3+}-Rich Cobalt Selenide Derived from ZIF-67 for Efficient Electrochemical Water Oxidation. *ACS Appl. Mater. Interfaces* **2016**, *8*, 20534−20539.
(26) Aijaz, A.; Masa, J.; Rösler, C.; Xia, W.; Weide, P.; Botz, A. J. R.; Fischer, R. A.; Schuhmann, W.; Muhler, M. Co@Co_3O_4 Encapsulated in Carbon Nanotube-Grafted Nitrogen-Doped Carbon Polyhedra as an Advanced Bifunctional Oxygen Electrode. *Angew. Chem., Int. Ed.* **2016**, *55*, 4087−4091.

(27) Xie, J.; Miao, Y.; Liu, B.; Shao, S.; Zhang, X.; Sun, Z.; Xu, X.; Yao, Y.; Hu, C.; Zou, J. CoFe Alloy-Coupled Mo_2C Wrapped by Nitrogen-Doped Carbon as Highly Active Electrocatalysts for Oxygen Reduction/Evolution Reactions. *Nanomaterials* **2023**, *13*, 543.
(28) Yi, Y.; Weinberg, G.; Prenzel, M.; Greiner, M.; Heumann, S.; Becker, S.; Schlögl, R. Electrochemical Corrosion of a Glassy Carbon Electrode. *Catal. Today* **2017**, *295*, 32−40.
(29) Möller, S.; Barwe, S.; Masa, J.; Wintrich, D.; Seisel, S.; Baltruschat, H.; Schuhmann, W. Online Monitoring of Electrochemical Carbon Corrosion in Alkaline Electrolytes by Differential Electrochemical Mass Spectrometry. *Angew. Chem., Int. Ed.* **2020**, *59*, 1585−1589.
(30) Ji, S. G.; Kim, H.; Lee, W. H.; Oh, H.-S.; Choi, C. H. Real-Time Monitoring of Electrochemical Carbon Corrosion in Alkaline Media. *J. Mater. Chem. A* **2021**, *9*, 19834−19839.
(31) Wu, T.; Han, M.; Zhu, X.; Wang, G.; Zhang, H.; Zhao, H. The Electrochemical Corrosion of an Air Thermally-Treated Carbon Fiber Cloth Electrocatalyst with Outstanding Oxygen Evolution Activity under Alkaline Conditions. *Chem. Commun.* **2019**, *55*, 2344−2347.
(32) Sato, Y.; Kowalski, D.; Aoki, Y.; Habazaki, H. Long-Term Durability of Platelet-Type Carbon Nanofibers for OER and ORR in Highly Alkaline Media. *Appl. Catal. Gen.* **2020**, *597*, 117555.
(33) Wu, X.; Zhao, K.; Yan, X.; Cao, X.; Ke, L.; Zhao, Y.; Li, L.; Jiang, X.; Yan, N. Suppressing Carbon Corrosion *via* Mechanically Mixing Transition Metal Phosphide Clusters: A Comparative *in Situ* Study in Alkaline Media. *J. Mater. Chem. A* **2023**, *11*, 17237−17245.
(34) Zeradjanin, A. R. The Era of Stable Electrocatalysis. *Nat. Catal.* **2023**, *6*, 458−459.
(35) Ross, P. N.; Sattler, M. The Corrosion of Carbon Black Anodes in Alkaline Electrolyte: III. The Effect of Graphitization on the Corrosion Resistance of Furnace Blacks. *J. Electrochem. Soc.* **1988**, *135*, 1464−1470.
(36) Persson, K. A.; Waldwick, B.; Lazic, P.; Ceder, G. Prediction of Solid-Aqueous Equilibria: Scheme to Combine First-Principles Calculations of Solids with Experimental Aqueous States. *Phys. Rev. B* **2012**, *85*, 235438.
(37) Singh, A. K.; Zhou, L.; Shinde, A.; Suram, S. K.; Montoya, J. H.; Winston, D.; Gregoire, J. M.; Persson, K. A. Electrochemical Stability of Metastable Materials. *Chem. Mater.* **2017**, *29*, 10159−10167.
(38) Jain, A.; Ong, S. P.; Hautier, G.; Chen, W.; Richards, W. D.; Dacek, S.; Cholia, S.; Gunter, D.; Skinner, D.; Ceder, G.; Persson, K. A. Commentary: The Materials Project: A Materials Genome Approach to Accelerating Materials Innovation. *APL Mater.* **2013**, *1*, 011002.
(39) Arikado, T.; Iwakura, C.; Yoneyama, H.; Tamura, H. The Anodic Polarization Characteristics of the Graphite in Alkaline Solution. *Electrochim. Acta* **1976**, *21*, 551−555.
(40) Nakahara, M.; Shimizu, K. Effects of Electrolyte on the Structure of Pyrolytic Graphite Surfaces in Anodic Oxidation. *J. Mater. Sci.* **1992**, *27*, 1207−1211.
(41) Ahn, S.; Tatarchuk, B. J.; Kerby, M. C.; Davis, S. M. Selective Electrochemical Oxidation of Coal in Aqueous Alkaline Electrolyte. *J. Electrochem. Soc.* **1995**, *142*, 782−787.
(42) Zuleta, M.; Björnbom, P.; Lundblad, A. Effects of Pore Surface Oxidation on Electrochemical and Mass-Transport Properties of Nanoporous Carbon. *J. Electrochem. Soc.* **2005**, *152*, A270.
(43) Filimonenkov, I. S.; Bouillet, C.; Kéranguéven, G.; Simonov, P. A.; Tsirlina, G. A.; Savinova, E. R. Carbon Materials as Additives to the OER Catalysts: RRDE Study of Carbon Corrosion at High Anodic Potentials. *Electrochim. Acta* **2019**, *321*, 134657.
(44) Li, Z. Q.; Lu, C. J.; Xia, Z. P.; Zhou, Y.; Luo, Z. X-Ray Diffraction Patterns of Graphite and Turbostratic Carbon. *Carbon* **2007**, *45*, 1686−1695.
(45) Cherstiouk, O. V.; Simonov, A. N.; Moseva, N. S.; Cherepanova, S. V.; Simonov, P. A.; Zaikovskii, V. I.; Savinova, E. R. Microstructure Effects on the Electrochemical Corrosion of Carbon Materials and Carbon-Supported Pt Catalysts. *Electrochim. Acta* **2010**, *55*, 8453−8460.
(46) Alegre, C.; Sebastián, D.; Lázaro, M. J. Carbon Xerogels Electrochemical Oxidation and Correlation with Their Physico-Chemical Properties. *Carbon* **2019**, *144*, 382−394.
(47) Pérez-Rodríguez, S.; Sebastián, D.; Lázaro, M. J. Electrochemical Oxidation of Ordered Mesoporous Carbons and the Influence of Graphitization. *Electrochim. Acta* **2019**, *303*, 167−175.
(48) Han, G.-F.; Xiao, B.-B.; Kim, S.-J.; Li, F.; Ahmad, I.; Jeon, I.-Y.; Baek, J.-B. Tuning Edge-Oxygenated Groups on Graphitic Carbon Materials against Corrosion. *Nano Energy* **2019**, *66*, 104112.
(49) Sato, Y.; Yamada, N.; Kitano, S.; Kowalski, D.; Aoki, Y.; Habazaki, H. High-Corrosion-Resistance Mechanism of Graphitized Platelet-Type Carbon Nanofibers in the OER in a Concentrated Alkaline Electrolyte. *J. Mater. Chem. A* **2022**, *10*, 8208−8217.
(50) Yang, J.; Park, S.; Choi, K. Y.; Park, H.-S.; Cho, Y.-G.; Ko, H.; Song, H.-K. Activity-Durability Coincidence of Oxygen Evolution Reaction in the Presence of Carbon Corrosion: Case Study of $MnCo_2O_4$ Spinel with Carbon Black. *ACS Sustain. Chem. Eng.* **2018**, *6*, 9566−9571.
(51) Baltruschat, H. Differential Electrochemical Mass Spectrometry. *J. Am. Soc. Mass Spectrom.* **2004**, *15*, 1693−1706.
(52) Chen, W.; He, F.; Chen, Y.-X. On the Accurate Calibration of Differential Electrochemical Mass Spectrometry. *Curr. Opin. Electrochem.* **2023**, *42*, 101393.
(53) Grey, L. H.; Nie, H.-Y.; Biesinger, M. C. Defining the Nature of Adventitious Carbon and Improving Its Merit as a Charge Correction Reference for XPS. *Appl. Surf. Sci.* **2024**, *653*, 159319.
(54) Ortiz Peña, N.; Ihiawakrim, D.; Han, M.; Lassalle-Kaiser, B.; Carenco, S.; Sanchez, C.; Laberty-Robert, C.; Portehault, D.; Ersen, O. Morphological and Structural Evolution of Co_3O_4 Nanoparticles Revealed by *in Situ* Electrochemical Transmission Electron Microscopy during Electrocatalytic Water Oxidation. *ACS Nano* **2019**, *13*, 11372−11381.
(55) Qu, J.; Sui, M.; Li, R. Recent Advances in In-Situ Transmission Electron Microscopy Techniques for Heterogeneous Catalysis. *iScience* **2023**, *26*, 107072.
(56) Sekar, A.; Yadav, R.; Basavaraj, N. Fluorescence Quenching Mechanism and the Application of Green Carbon Nanodots in the Detection of Heavy Metal Ions: A Review. *New J. Chem.* **2021**, *45*, 2326−2360.
(57) Grindlay, G.; Mora, J.; De Loos-Vollebregt, M.; Vanhaecke, F. A Systematic Study on the Influence of Carbon on the Behavior of Hard-to-Ionize Elements in Inductively Coupled Plasma-Mass Spectrometry. *Spectrochim. Acta Part B At. Spectrosc.* **2013**, *86*, 42−49.
(58) Provin, T. Chapter 5.2 Total Carbon and Nitrogen and Organic Carbon via Thermal Combustion Analyses. In *Soil Test Methods From the Southeastern United States*; SERA-IEG-6, 2014; pp 149-154.
(59) Pan, Y.; Cheng, X.; Gong, L.; Shi, L.; Deng, Y.; Zhang, H. Highly Reversible Na Ion Storage in N-Doped Polyhedral Carbon-Coated Transition-Metal Chalcogenides by Optimizing the Nanostructure and Surface Engineering. *J. Mater. Chem. A* **2018**, *6*, 18967−18978.
(60) Hu, J.; Peng, L.; Primo, A.; Albero, J.; García, H. High-Current Water Electrolysis Performance of Metal Phosphides Grafted on Porous 3D N-Doped Graphene Prepared without Using Phosphine. *Cell Rep. Phys. Sci.* **2022**, *3*, 100873.
(61) Li, Y.; Wei, B.; Yu, Z.; Bondarchuk, O.; Araujo, A.; Amorim, I.; Zhang, N.; Xu, J.; Neves, I. C.; Liu, L. Bifunctional Porous Cobalt Phosphide Foam for High-Current-Density Alkaline Water Electrolysis with 4000-h Long Stability. *ACS Sustain. Chem. Eng.* **2020**, *8*, 10193−10200.
(62) Chen, F.-Y.; Wu, Z.-Y.; Adler, Z.; Wang, H. Stability Challenges of Electrocatalytic Oxygen Evolution Reaction: From Mechanistic Understanding to Reactor Design. *Joule* **2021**, *5*, 1704−1731.
(63) Terlouw, T.; Bauer, C.; McKenna, R.; Mazzotti, M. Large-Scale Hydrogen Production *via* Water Electrolysis: A Techno-Economic and Environmental Assessment. *Energy Environ. Sci.* **2022**, *15*, 3583−3602.
(64) Marquez, R. A.; Espinosa, M.; Kalokowski, E.; Son, Y. J.; Kawashima, K.; Le, T. V.; Chukwuneke, C. E.; Mullins, C. B. A Guide to Electrocatalyst Stability Using Lab-Scale Alkaline Water Electrolyzers. *ACS Energy Lett.* **2024**, *9*, 547−555.

https://doi.org/10.1021/acsmaterialslett.4c00688
ACS Materials Lett. 2024, 6, 3190−3201

(65) El Mrabet, R.; Berrada, A. Hydrogen Production and Derivatives from Renewable Energy Systems for a Best Valorization of Sustainable Resources. In *Hybrid Energy System Models*; Elsevier, 2021; pp 343-363. DOI: 10.1016/B978-0-12-821403-9.00010-X.
(66) Zhao, J.; Huang, X.; Chang, H.; Hwa Chan, S.; Tu, Z. Effects of Operating Temperature on the Carbon Corrosion in a Proton Exchange Membrane Fuel Cell under High Current Density. *Energy Convers. Manag. X* **2021**, *10*, 100087.
(67) Jiang, H.; Gu, J.; Zheng, X.; Liu, M.; Qiu, X.; Wang, L.; Li, W.; Chen, Z.; Ji, X.; Li, J. Defect-Rich and Ultrathin N Doped Carbon Nanosheets as Advanced Trifunctional Metal-Free Electrocatalysts for the ORR, OER and HER. *Energy Environ. Sci.* **2019**, *12*, 322−333.
(68) Li, Y.; Lu, J. Metal-Air Batteries: Will They Be the Future Electrochemical Energy Storage Device of Choice? *ACS Energy Lett.* **2017**, *2*, 1370−1377.
(69) Peng, C.; Chen, J.; Jin, M.; Bi, X.; Yi, C.; Zhang, S.; Xu, X.; Liu, W.; Liu, X.; Lai, L. Effect of the Carbon on the Electrochemical Performance of Rechargeable Zn-Air Batteries. *Int. J. Hydrog. Energy* **2023**, *48*, 5313−5322.

https://doi.org/10.1021/acsmaterialslett.4c00688
ACS Materials Lett. 2024, 6, 3190−3201